

1 **Morphology and size of the particles emitted from a gasoline**
2 **direct injection-engine vehicle and their ageing in an**
3 **environmental chamber**

4
5 Jiaoping Xing^{a,b}, Longyi Shao^{a*}, Wenbin Zhang^c, Jianfei Peng^d, Wenhua wang^a, Shijin
6 Shuai^c, Min Hu^d, Daizhou Zhang^{e*}

7
8 ^aState Key Laboratory of Coal Resources and Safe Mining, School of Geoscience and Survey
9 Engineering, China University of Mining and Technology (Beijing), Beijing 100083, China.

10 ^b2011 Collaborative Innovation Center of Jiangxi Typical Trees Cultivation and Utilization, School of
11 Forestry, Jiangxi Agricultural University, Nanchang, 330045, China.

12 ^cState Key Laboratory of Automotive Safety and Energy, Department of Automotive Engineering,
13 Tsinghua University, Beijing 100084, China

14 ^dState Key Joint Laboratory of Environmental Simulation and Pollution Control, College of
15 Environmental Sciences and Engineering, Peking University, Beijing 100871, China

16 ^eFaculty of Environmental and Symbiotic Sciences, Prefectural University of Kumamoto, Kumamoto
17 862-8502, Japan

18
19 * Corresponding Author - e-mail: shaoL@cumtb.edu.cn (Longyi Shao); dzzhang@pu-kumamoto.ac.jp
20 (Daizhou Zhang)

21
22
23 **Highlights**

- 24 1. GDI-engine vehicles emitted a large amount of both primary and secondary organic
25 aerosols.
- 26 2. Higher contents of organic particles were emitted under hot stabilized running and
27 hot start states.
- 28 3. Sulfate and secondary organic aerosol form on the surface of primary particles after
29 ageing.
- 30 4. Particles aged rapidly by catalyzed acidification under high pollution levels in
31 Beijing.

32
33
34

35 **Abstract:**

36 Air pollution is particularly severe in developing megacities, such as Beijing,
37 where vehicles equipped with modern gasoline direct injection (GDI) engines are
38 becoming one of major sources of the pollution. This study presents the characteristics
39 of individual particles emitted by a GDI gasoline vehicle and their ageing in a smog
40 chamber under the Beijing urban environment, as part of the Atmospheric Pollution &
41 Human Health (APHH) research programme. Using transmission electron microscopy,
42 we identified the particles emitted from a commercial GDI-engine vehicle running
43 under various conditions, namely, cold start, hot start, hot stabilized running, idle, and
44 acceleration states. Our results show that most of the particles were organic, soot and
45 Ca-rich ones, with small quantities of S-rich and metal-containing particles. In terms of
46 particle size, the particles exhibited a bimodal distribution in number *vs* size, with one
47 mode at 800–900 nm, and the other at 140–240 nm. The amounts of organic particles
48 emitted under hot start and hot stabilized states were higher than those emitted under
49 other conditions. The amount of soot particles was higher under cold start and
50 acceleration states. Under the idle state, the proportion of Ca-rich particles was highest,
51 although their absolute number was low. In addition to quantifying the types of particles
52 emitted by the engine, we studied the ageing of the particles during 3.5 hours of
53 photochemical oxidation in an environmental chamber under the Beijing urban
54 environment. Ageing transformed soot particles into core-shell structures, coated by
55 secondary organic species, while the content of sulfur in Ca-rich and organic particles
56 increased. Overall, the majority of particles from GDI-engine vehicles are organic and

57 soot particles with submicron or nanometric size. The particles are highly reactive; they
58 react in the atmosphere and change their morphology and composition within hours via
59 catalyzed acidification that involves gaseous pollutants at high pollution levels in
60 Beijing.

61

62 **1. Introduction**

63 Air pollution caused by PM_{2.5} in megacities such as Beijing, the capital city of
64 China, is of public and academic concerns due to its environmental impacts (Bond et
65 al., 2013; Liu et al., 2017; Huang et al., 2014) and adverse health effects (Shao et al.,
66 2017; Chart-asa and Gibson, 2015). Motor vehicle emissions are one of the most
67 significant sources of airborne particles in the urban atmosphere (Hwa and Yu, 2014),
68 and contribute up to 31% of primary particulate emissions of PM_{2.5} in Beijing (Yu et
69 al., 2013). Moreover, secondary aerosol formation associated with traffic emissions is
70 a major process leading to the rapid increase of PM_{2.5}, which results in severe haze
71 episodes (Huang et al., 2014). Although emissions from gasoline engines are relatively
72 lower than those from diesel engines (Alves et al., 2015), the number of gasoline-
73 powered vehicles in urban areas greatly exceeds that of diesel-powered vehicles. The
74 total number of vehicles in China reached 310 million in 2017, about 70% of these were
75 powered by gasoline engines (National Bureau of Statistics of China, 2018). There are
76 two main types of gasoline engines, namely, conventional multipoint port fuel injection
77 (PFI) engines and gasoline direct injection (GDI) engines. In recent years, the demand
78 for engines with high efficiency and low fuel consumption has led to an increasing use

79 of GDI engines in light-duty passenger cars. The market share of GDI-engine vehicles
80 has increased dramatically over the past decade and was estimated to reach 50% of new
81 gasoline vehicles sold in 2016 (Zimmerman et al., 2016). In Beijing and northern China,
82 the vehicle emissions become a more concerning issue in terms of air pollution when
83 the emission from coal combustion are seriously reduced after the Action for
84 Comprehensive Control of Air Pollution in Beijing since 2017 (Chang et al., 2019;
85 Chen et al. 2019; Zhang et al. 2019). In spite of this, regional transport of coal-burning
86 emissions from the surrounding areas can still influence the urban air sometimes
87 severely in winter (Ma et al., 2017; Zhang et al., 2019).

88 The number, mass and size distribution of particles emitted from GDI-engine
89 vehicles have been studied (Khalek et al., 2010; Maricq et al., 2011; Baral et al., 2011).
90 The size distribution usually has an accumulation mode with the maxima in the
91 diameter range of 100–300 nm. Major components of the particles include elemental
92 carbon (EC), organic carbon, and ash (Giechaskiel et al., 2014). Besides particulate
93 matter, the engines emit gaseous hydrocarbon compounds. These compounds might
94 form particles, or be adsorbed on the surface of particle aggregates, leading to the
95 growth of the particles in the engine emission (Luo et al., 2015). Relatively high particle
96 emissions by GDI-engine vehicles have prompted studies on the effects of engine
97 operating parameters and fuel composition on the characteristics of the particles (Hedge
98 et al., 2011; Szybist et al., 2011). It has been found that, in general, emissions under the
99 cold start condition make up the major contribution to the total amount of PM emissions
100 from GDI engines (Chen and Stone, 2011). Studies have also demonstrated that the

101 highest particle emissions from GDI engines in number concentration occur under the
102 acceleration state during transient vehicle operations (Chen et al., 2017).

103 Studies have also shown that gasoline vehicles are an important source of
104 secondary aerosol precursors in urban areas (Suarez-Bertoa et al., 2015). Secondary
105 aerosols can be formed via gas-phase reactions of volatile organic compounds and
106 multiphase and heterogeneous processes of primary particles (Zhu et al., 2017).
107 Experiments performed in environmental chambers demonstrated that the mass of
108 secondary aerosols derived from precursors could exceed that of directly-emitted
109 aerosols (Jathar et al., 2014). The occurrence of secondary aerosols on particles could
110 change the properties of particles in size, mass, chemical composition, morphology,
111 optical and hygroscopic parameters. These changes, in turn, might affect the
112 environmental impact of the particles significantly, for instance in terms of visibility,
113 human health, weather, and energy budgets (Peng et al., 2017; Laskin et al., 2015). In
114 general, the ageing processes of primary particles in the atmosphere are studied to
115 understand their climate effects (Niu et al., 2011). However, the lack of data on primary
116 particles emitted by gasoline engines hinders a deep understanding of the roles and
117 activities of the particles in ambient air pollution and relevant environmental effects.

118 Atmospheric Pollution & Human Health (APHH) research programme aimed to
119 explore the sources and processes affecting urban atmospheric pollution in Beijing.
120 Details regarding this project are given in Shi et al. (2018). To address one of the aims
121 of the AIRPOLL-Beijing (Source and Emissions of Air Pollutants) and AIRPRO-
122 Beijing (The integrated Study of AIR Pollution Processes), we employed a dedicated

123 experiment to investigate the characteristics of the individual particles, in terms of the
124 number concentration, size distribution, emitted from a GDI-engine vehicle during a
125 real-world driving cycle for chassis dynamometer test, i.e., the Beijing driving cycle
126 (BDC). Various test modes were introduced to accurately evaluate the emission from
127 light- or medium-duty vehicles. Furthermore, experiments were conducted in an
128 environmental chamber to investigate the ageing processes of particles emitted by GDI-
129 engine vehicles in ambient air in Beijing. We utilized a transmission electron
130 microscope equipped with an Oxford energy-dispersive X-ray spectrometer (TEM-
131 EDX) to identify the morphology, size and elemental composition of particles emitted
132 by the GDI-engine vehicle when it was running under different states. Particles before
133 and after a 3.5-hour ageing in the chamber were compared on the basis of the TEM-
134 EDX analysis. The TEM-EDX analysis provides the information on the internal
135 inhomogeneity, mixing state and surface characteristics of individual particles and has
136 been used to analyze the aerosol particles (Li and Shao, 2009; Shao et al., 2017; Adachi
137 and Buseck, 2015; Loh et al., 2012). The experimental design allows for the study of
138 the physical and chemical characteristics of the particles emitted from the GDI-engine
139 vehicles, as well as their ageing in a simulated urban atmosphere. The purposes of this
140 study are to evaluate the individual characteristics and the ageing process of primary
141 particles emitted by a GDI-engine vehicle, to investigate the ageing processes of such
142 particles in the atmosphere, and to deepen the understanding of the environmental
143 impact of gasoline-powered vehicle emissions.

144 **2. Material and methods**

145 **2.1 Test vehicle, fuels, and test procedure**

146 The GDI-engine vehicle utilized in the experiment complies with the China Phase
147 4 (equivalent to Euro 4) standard. It uses a three-way catalyst to reduce gaseous
148 emissions. The GDI (model GDI-1.4-T) in the test vehicle is recognized as a
149 representative of leading-edge designs of gasoline engines, because of its advanced
150 engine technologies such as its better fuel burning efficiency and lower greenhouse gas
151 emissions than other types of engine. Vehicles equipped with such GDI engines
152 constitute the majority of light-duty vehicles in China, especially in large cities like
153 Beijing. Details of the engine used in this study are listed in Table S1. The fuel used in
154 the experiment is a commercial gasoline blend of common quality in China. The
155 properties of the fuel were measured by SGS-CSTC Standards Technical Services Co.,
156 Ltd., China, and are listed in Table S2. The fuel has a Research Octane Number (RON)
157 of 93 and is a fifth-stage gasoline. It contains 36.7% of aromatics and 15.4% of olefins
158 in volume and has 6% of sulfur in mass, representing a typical fifth-stage gasoline in
159 China (with high aromatics) and is now widely used in Beijing. The experiments were
160 conducted within repeated Beijing Driving Cycles (BDCs), and one BCD included a
161 200-s “cold start” phase followed by an 867-s “hot stabilized running” phase. The
162 conditions during a BDC in the experiments are illustrated in Figure S1a. The cold start
163 state was achieved by starting the vehicle with a period of small accelerations, while
164 the hot stabilized running state had multiple periods of large acceleration and a
165 maximum velocity of 50 km h⁻¹. The BDC, characterized by a higher proportion of
166 idling periods and a lower acceleration speed than the New European Driving Cycle

167 (NEDC), was performed to simulate the repeated braking and acceleration on road in
168 megacities such as Beijing.

169 All tests were performed on a Euro 5/LEV2/Tier 2-capable test cell on a 48-inch
170 single-roll chassis dynamometer at the State Key Laboratory of Automobile Safety and
171 Energy Conservation at Tsinghua University. The test procedure for each run was as
172 follows: fuel change, BDC preparation, soak, cold start BDC test, and hot start BDC
173 test. After fuel change and BDC preparation, the test vehicle was then conditioned with
174 an overnight soak for more than 10 h. The soak room temperature was maintained
175 between 20 and 30 °C. Due to the limitation of the facilities and available running time,
176 a hot start test was conducted within 5 mins after the cold start test. A dilution unit was
177 applied to dilute the exhaust from the tailpipe into 1/10 in volume using synthetic air
178 composed of 79% N₂ and 20% O₂, in order to obtain the concentrations suitable for
179 subsequent measurements and suppress possible coagulation. The number
180 concentration of the emitted particles was monitored by a Combustion Fast Particle
181 Size Spectrometer Differential Mobility Spectrometer 500 (DMS 500). The maximum
182 measurable number concentration of DMS 500 was 10¹¹ (dN/dlogDp/cc) after the
183 dilution (Petzold et al., 2011). For the analyses of individual particles, 6–8 samples
184 were collected during one BDC test. At least one sample was collected under each
185 running state (i.e. cold start, hot start, idle state, acceleration state, or hot stabilized
186 running state). The driving cycle test was repeated at least twice. Two or more samples
187 were obtained for each running state. A single-stage cascade impactor (KB-2, Qingdao
188 Jinshida Company) was mounted to the exit of the tailpipe after the dilution unit. The

189 emitted particles were collected onto 300-mesh copper TEM grids, which were covered
190 with a carbon-coated formvar film. The flow rate was 1.0 L min^{-1} , and the cut-off
191 diameter of the impactor for 50% collection efficiency was $0.25 \text{ }\mu\text{m}$ if the density of
192 the particles was 2 g cm^{-3} . For each sample, the collection time was 60 s.

193 **2.2 Environmental chamber experiments**

194 Particles from the GDI-engine vehicle were introduced into an environmental
195 chamber and exposed to sunlight. The chamber, made of perfluoroalkoxy (PFA) Teflon
196 in order to achieve a high transmission of ultraviolet light, had an internal volume of
197 1.2 m^3 . Ambient sunlight was used as the driving force for photochemical reactions in
198 the chamber, in an environment close to actual open air. Before the experiments, the
199 chamber was cleaned by flushing with zero air for approximately 12 hours and
200 illuminated with sunlight, to remove residues that could influence the experiments.
201 H_2O_2 (1 mL, 30%), together with the vehicle emission, was injected into the chamber
202 to generate OH exposure. Assuming the 24 hr mean concentration of 10^6 OH molecules
203 cm^{-3} in Beijing (Lu et al., 2013), the OH exposure at the end of the experiments
204 reproduced extreme oxidation processes in the atmosphere, which is equivalent to cases
205 of an oxidation more than 10 days. The aging experiments for the gasoline exhausts
206 were carried out with a relatively high OH exposure compared to ambient conditions in
207 order to obtain the aging process. This method and the amount of H_2O_2 have been
208 frequently used in smog chamber experiments (Song et al., 2007; Song et al., 2019).
209 After the injection, the experiments were conducted from approximately 13:00 to 17:00
210 local time under sunshine, with the relative humidity being kept at around 50%. The
211 global solar radiation when the tests were carried out was approximately 318 W m^{-2} .

212 After 3.5 h of ageing, the particles in the chamber were collected onto mesh TEM grids
213 using the impactor. The collection time for each sample was 120 s. The schematic
214 diagram of the experimental system is presented in Figure S1b.

215

216 **2.3 TEM/EDX and scanning transmission electron microscopy (STEM) analyses**

217 The particles in the samples were examined using a Tecnai G2 F30 field emission
218 high-resolution transmission electron microscope (FE-HRTEM). This microscope is
219 also equipped with an Oxford EDX and a STEM unit with a high-angle annular dark-
220 field detector (HAADF). The EDX can detect elements with the atom number larger
221 than 5 (B) in a single particle. The HAADF can detect the distribution of a certain
222 element by mapping the distribution of the element in a particle. The TEM was operated
223 with the acceleration voltage of 300 kV. EDX spectra were firstly collected for 20 live
224 seconds to minimize the influence of radiation exposure and potential beam damage
225 and then for 90 live seconds for a range of possible elements. Copper was excluded
226 from the analysis because of interference from the TEM grids which are made of copper.

227 To ensure the representativeness of the analyzed particles, more than 150 particles
228 from at least 3 random areas were analyzed from the center and periphery of the
229 sampling spot on each grid. All individual particles larger than 50 nm in the selected
230 areas were analyzed. The TEM images were digitized using an automated fringe image
231 processing system named Microscopic Particle Size of Digital Image Analysis System
232 (UK) to project the surface areas of the particles. The equivalent spherical diameter of
233 a particle was calculated from its projected area, expressed as the square root of $4A/\pi$,
234 where A is the projected area. The electron microscope analysis of individual particles

235 is very time consuming, which hindered us from analyzing more particles from multiple
236 engines emission.

237 **3. Results**

238 **3.1. Particle morphology, elemental composition and size**

239 A total of 2880 particles were analyzed from the GDI-engine vehicles. Most of the
240 particles were in the sub-micrometer size range. Based on morphology and elemental
241 composition of the particles, the majority of them were identified as soot, organic and
242 Ca-rich particles, a smaller amount was identified as S-rich or metal-rich particles (Fig.
243 1). The method of particle classification is similar to that adopted by Okada et al. (2005)
244 and Xing et al. (2019). In the following description, “X-rich” means that the element
245 “X” occupies the largest proportion in the element composition of the particles. Figure
246 2 illustrates the number-size distributions of the relative concentration ($dN/d\log D$) of
247 primary particles from the GDI-engine vehicle, where N is the relative number fraction
248 and D is the equivalent diameter. The particles were in the range of 60–2500 nm and
249 displayed a bimodal distribution, with one mode in the 140–240 nm range, and another
250 in the 800–900 nm range. Particles smaller than 250 nm were largely underestimated
251 because of the loss during the particle collection. Therefore, there should have been
252 more particles in the smaller mode range than shown in Figure 2. Concerning the loss
253 of small particles, we measured the size distribution by the DMS500 (Fig. S2). The
254 results showed that a large amount of nucleation mode particles were emitted by the
255 GDI vehicle.

256 It should be noted that organic particles were mainly composed of C and O
257 elements, and contained a small amount of inorganic elements Ca, P, S and Zn.

258 Elemental mapping of the organic particles exhibited the presence of Ca, P, S and Zn in
259 some of the particles, showing the mixture state of organic and inorganic materials (Fig.
260 1f). It has been reported that such particles could be related to the combustion of fuels
261 or lubrication oil (Rönkkö et al., 2013). In addition to these primary organic particles,
262 the GDI-engine vehicle emitted precursor gases, which produced secondary organic
263 particles via gas-phase reactions, and multiphase and heterogeneous processes on the
264 primary particles. A group of spherical particles were found in the environmental
265 chamber (Fig. 1g). These particles became semi-transparent or transparent to an
266 electron beam, which is characteristic of organic materials, liquid water, or their
267 evaporation residues either mixed or not mixed with electron absorptive materials. We
268 regard these particles as secondary organic particles because the humidity in the
269 chamber during the experiment was kept much below saturation (relative humidity
270 around 50%). Therefore, these particles were expected to mainly consist of secondary
271 organic materials, which should have been produced via gas phase reactions or on the
272 surface of pre-existing particles (Hu et al., 2016). No other elements, except C and O,
273 were identified in these particles, which is consistent with the above inference. Similar
274 particles were also encountered in other environmental chamber experiments studying
275 emissions from light-duty gasoline vehicles (Jathar et al., 2014).

276

277 **3.2 Number fractions of particles**

278 Figure 3 illustrates the numbers of accumulation mode particles emitted by
279 burning one kilogram of fuel during the cold start and hot start driving cycles. PM
280 emissions at the start-up stage under both cold and hot start states were higher than the

281 emissions under the states when the engine was fully warmed and the vehicle operation
282 was stabilized. The PM emission was the highest under the hot stabilized running state
283 (2.3×10^{10} particles (kg fuel)⁻¹), followed by those under the hot start (1.2×10^{10} particles
284 (kg fuel)⁻¹), cold start (7.1×10^9 particles (kg fuel)⁻¹), and acceleration running states
285 (2.9×10^9 particles (kg fuel)⁻¹), with the emission under the idle running state being the
286 lowest (7.4×10^8 particles (kg fuel)⁻¹) (Fig. S3). Size distributions of the particles varied
287 with driving conditions (Fig. S4). Under the cold start state and acceleration running
288 state, higher number concentrations, and thus higher mass concentrations of the
289 particles with accumulation mode were emitted in comparison with other running states.

290 Under all the running states, morphologies and types of the particles remained
291 similar but the proportions of different types of particles differed considerably (Fig. S5).
292 The proportion of organic particles was high under hot stabilized and hot start states.
293 Soot particles were abundant under cold start and acceleration states. A relatively higher
294 proportion of Ca-rich particles was found under idle state, compared to those under
295 other running states.

296 We estimated the number of different type particles in the emission under the
297 running states by burning one kilogram of fuel (Fig. 4). Organic particles in the
298 emission under the hot stabilized running state (2.3×10^9 particles (kg fuel)⁻¹) and the
299 hot start running state (3.6×10^8 particles (kg fuel)⁻¹) were higher than in the emission
300 under other running states. The number of soot particles were higher under the hot
301 stabilized running state (1.7×10^9 particles (kg fuel)⁻¹) and the cold start state (5.9×10^8
302 particles (kg fuel)⁻¹) than those under other running states. Under the idle state, the

303 relative proportion of Ca-rich particles was the highest, although their absolute number
304 was low (1.4×10^9 particles (kg fuel)⁻¹).

305 Under the cold start state, a significant proportion of the emitted particles were
306 soot particles. This can be attributed to the incomplete vaporization of fuel droplets in
307 the combustion cylinder (Chen et al., 2017). Under the hot start state and the hot
308 stabilized running state, organic particles were predominant. Under these two running
309 states, the engine temperature was high, which enabled the fuel to evaporate and mix
310 with the air easily. With the increase of the temperature in the cylinders, the rate of
311 particle oxidation increased, which could cause an increase of organic particles in the
312 emission (Fu et al., 2014). Under the idle state, the fuel consumption was much lower
313 than that under the other running states, which resulted in a higher relative contribution
314 to particles from lubricant oil. The high Ca content in the lubricant oil led to a higher
315 Ca-rich particle emission under this running state. Under the acceleration state, the
316 predominant types of particle included soot, organic, and Ca-rich particles. As the
317 acceleration running required a high vehicular speed and engine load, the emissions
318 contained more soot particles than those under other running states.

319 **3.3. Aged particles in the environmental chamber**

320 A large amount of secondary organic particles (accounting for 80%-85% in
321 number), some soot particles, Ca-rich particles, and primary organic particles were
322 detected in the environmental chamber (Fig. 5). After the ageing process, many soot
323 particles changed into core-shell structures and became coated with secondary species
324 (Figs. 5b and 5c). The EDX results showed that almost all coatings were mainly
325 composed of C, O, and S, suggesting these coatings were a mixture of organic and

326 sulfate. The morphology and compositions of Ca-rich particles and organic particles
327 (Figs. 5e and 5g) changed, with the aged ones having a more irregular shape and a
328 higher sulfur content in comparison with fresh ones (Figs. 5A and B).

329 Approximately 80% of the soot particles were present in core-shell structures and
330 coated with secondary species after the 3.5-hour ageing. In contrast, before the ageing,
331 the particles with a core-shell structure were only about 10% of the total. The mean
332 diameter of the soot particles after ageing was around 0.49 μm , which was much smaller
333 than that before the ageing (0.65 μm), indicating the shrinkage of the soot particles
334 during the ageing (Fig. 5b). The core-shell ratios, defined as the ratio of the diameter of
335 the core part (D_{core}) to the diameter of the whole particle (D_{shell}) (Niu et al., 2016;
336 Hou et al., 2018), were used to quantify the aging degree of the soot particles with
337 coating. It was found that the core-shell ratios of the soot particles in the smog chamber
338 were mainly in the range of 0.25–0.78, indicating the stronger aging degree of soot
339 particles in the chamber than case data in urban air with the ratios of 0.4–0.9 (Niu et al.,
340 2016).”

341 **4. Discussion**

342 **4.1. Contribution of GDI-engine vehicle emissions to urban air pollution**

343 Our investigation shows that the GDI-engine vehicle emitted a large amount of
344 organic particles (32%), soot (32%), Ca-rich particles (26%), S-rich (5%) and metal-
345 containing particles (4%). Relevant studies have also shown that the primary
346 carbonaceous aerosols (element carbon + primary organic aerosol) accounted for 85 %
347 of the PM in the GDI vehicles, suggesting that carbonaceous aerosols were the major

348 contributors in the PM from GDI gasoline vehicles (Du et al., 2018). Considering the
349 large fraction of the vehicles equipped with GDI engines in megacities like Beijing, this
350 indicates a possible substantial contribution of GDI-engine vehicles to urban air
351 pollution. Moreover, organic particles occupied the majority of the particles emitted
352 under hot stabilized running and hot start states. It has been noted that the organic matter
353 was the major component of the total particle mass during the hot start conditions (Chen
354 et al., 2017; Fushimi et al., 2016), which is consistent with the results obtained for the
355 number concentrations in our study. The hot stabilized running state is the most
356 frequent running condition of vehicles, whereas the hot start state is the most frequent
357 condition in congested traffic. This suggests that a substantial number of organic
358 compounds in the air pollution of populated cities might be directly related to vehicle
359 emissions.

360 Organic particles and soot particles in ambient air are emitted from a range of
361 sources including fossil fuels, biomass burning and urban waste burning (Kanakidou et
362 al., 2005). Table 1 shows the major characteristics of particles in the emissions from
363 different sources. For instance, there is a higher fraction of soot particles and a lower
364 fraction of organic particles in the emissions of GDI-engine vehicles compared to PFI-
365 engine vehicles (Xing et al., 2017). Organic particles in emissions from gasoline
366 vehicles are usually enriched in Ca, S and P (Liati et al., 2018; Xing et al., 2017). In
367 comparison, emissions from biomass/wood burning are usually dominated by organic
368 particles, which account for more than 50% of the total amount of particles (Liu et al.,
369 2017). Furthermore, organic particles from biomass/wood burning usually show

370 elevated K content, and thus, this element is frequently used as an indicator for
371 biomass/wood burning organic particles (Niu et al., 2016). Observations of primary
372 particles directly from coal burning have also demonstrated a predominance of organic
373 particles, soot particles, S-rich particles and mineral particles (Wang et al., 2019; Zhang
374 et al., 2018). Both biomass burning and coal combustion can produce organic particles
375 and almost all the emitted particles contain a certain amount of Si in addition to C and
376 O. Table 1 also shows the elemental concentrations in the organic particles in the
377 emissions from different types of sources. Since the concentrations of minor elements
378 in the organic particles are highly dependent on the sources, they could be used for
379 source identification of individual particles in the atmosphere.

380 The present data also permit the compilation of a rough inventory of particle
381 categories and amounts emitted from GDI-engine vehicles under various running
382 conditions (Fig. 4). Combined with statistics on the number of vehicles with GDI
383 engines, the running time and the running conditions on roads within a certain area, it
384 is possible to make an approximate estimate of the amounts of primary particles emitted
385 from GDI-engine vehicles. Such estimate is the basis for accurate source apportionment
386 of particles from vehicles, and it will be very beneficial for studies on the anthropogenic
387 sources of primary particles in urban air. These data could be brought together to better
388 understand the sources of air pollutants in the Beijing megacity and to improve the
389 capability of developing cost-effective mitigation measures.

390 **4.2 Rapid ageing of primary particles in Beijing**

391 The results of chamber experiments indicate that sulfate and secondary organic

392 aerosol (SOA) form on the surface of soot, Ca-rich and organic particles. Moreover, the
393 atmospheric transformation of primary particles emitted by the GDI-engine vehicles
394 could occur within 3.5 hours, indicating the ageing was rapid. Peng et al. (2014) found
395 similar timescales for black carbon transformation under polluted conditions in Beijing.
396 The rapid ageing of primary particles could be caused by several factors, such as the
397 concentration of gaseous pollutants from the vehicles, strength of solar radiation,
398 relative humidity (RH), and O₃ concentration (Guo et al., 2012; Deng et al., 2017; Du
399 et al., 2018). The present experiments were conducted in the atmosphere with relative
400 humidity of approximately 50% and solar radiation of 318 Wm⁻². The total hydrocarbon
401 emission (THC) from the GDI vehicles was 0.297 g km⁻¹. Repeated braking and
402 acceleration in the BDC could cause incomplete combustion and consequently high
403 THC emission. Under a high concentration of gaseous pollutants, primary particles
404 would age rapidly when exposed to solar radiation. Consequently, secondary species
405 including SOA and sulfate were produced on or condensed onto the particles, leading
406 to the coating. Guo et al. (2014) also showed that secondary photochemical growth of
407 fine aerosols during the initial stage of haze development could be attributed to highly
408 elevated levels of gaseous pollutants.

409 The mixture of SOA and sulfate have been detected in our chamber experiment,
410 indicating the involvement of inorganic salts in the SOA formation. Previous studies
411 have demonstrated the enhancement of SOA production in the presence of inorganic
412 sulfate (Beardsley and Jang, 2015; Kuwata et al., 2015), and this is because sulfate can
413 catalyze carbonyl heterogeneous reactions, and consequently, lead to SOA production

414 (Jang et al., 2002; Jang et al., 2004). Moreover, these aged primary particles favored
415 the formation of secondary aerosols by providing reaction sites and reaction catalysts.
416 Sulfate and secondary organic aerosol (SOA) co-existed on the surface of primary
417 particles, such as soot, Ca-rich and organic particles. In addition, the products of VOCs
418 oxidation could react with SO₂ to rapidly produce sulfate (Mauldin et al., 2012). Thus,
419 the rapid ageing of primary particles could also be attributable to the acid-catalyzed
420 mechanism. As the major source of pollutants in urban air, the GDI-engine vehicles
421 supply both primary particles and precursor gaseous species, and the rapid ageing of
422 the particles under certain conditions is very likely to be the major driving force for the
423 elevation of urban air pollution.

424 **4.3 Implications and perspectives**

425 Our results indicate that GDI-engine vehicles emitted a large amount of both
426 primary and secondary organic aerosols. PM number emission of organic particles from
427 GDI-engine vehicle were 2.9×10^9 particles (kg fuel)⁻¹ during the BDC. Secondary
428 organic particle was predominant in the secondary aerosols, accounting for 80-85%
429 particles in the chamber. Organic aerosols (OA) play an important role in the Earth's
430 radiation balance not only for its absorption and scattering of solar radiation but also
431 because they can alter the microphysical properties of clouds (Scott et al., 2014).
432 Particle size, shape, mixing state and composition affect their light scatterings and
433 absorption cross sections, and cloud condensation nuclei activity (Jacobson, 2001). OA
434 were composed of various types of chemical compounds with varying absorption
435 properties (mixing state), which were determined by the emission sources, the

436 formation mechanism (Zhu et al., 2017), and the source regions (Laskin et al., 2015).
437 Primary OA from biomass burning was co-emitted with soot (black carbon), inorganic
438 salts, and fly ash, producing internally and externally mixed particles in which the
439 organic components were present in different relative abundance (Lack et al., 2012).
440 Similarity, primary OA in the exhaust of gasoline and diesel vehicles were mixed with
441 Ca, P, Mg, Zn, Fe, S, and minor Sn inorganic compounds (Liati et al., 2018). In addition,
442 previous measurements indicated that SOA usually exists as an internal mixture with
443 other aerosols, such as sulfate, ammonium, or nitrate (Zhu et al., 2017). Our results
444 showed that the POA emitted from GDI-engine vehicle were mixed with soot, inorganic
445 components such as Ca, P, and Zn. Some of the SOA formed in the smog chamber were
446 mixed with sulfate. The complexity of mixing state makes it difficult to characterize the
447 properties of OA. Lang-Yona et al. (2010) found that for aerosols consisting of a
448 strongly absorbing core coated by a non-absorbing shell, and the Mie theory prediction
449 deviated from the measurements by up to 10%. Moreover, atmospheric aging process,
450 involving aqueous-phase aging and atmospheric oxidation, can either enhance or
451 reduce light absorption by OA (Bones et al., 2010). The condensation process may
452 result in a dramatic enhancement of hydrolysis of OA compounds, affecting their
453 absorption spectra (Lambe et al., 2015).

454 Our results also showed that primary organic aerosols (POA) emitted by GDI-
455 engine vehicles could acquire OA and sulfate coatings rapidly, within a few hours, and
456 increase a sizable fraction of total ambient aerosols existing as internal mixtures. In
457 addition, the fast ageing further caused the increase of aged POA in the total OA,

458 consequently, largely modified the properties of the particles such as their optical
459 properties. The results of the experiments in the chamber showed that most of the aged
460 POA had a core-shell structure, whereas most of the secondary organic aerosols (SOA)
461 produced by gas-phase reactions had a uniform structure. These results push forward
462 the understanding on the mixing state and chemical composition of both POA and SOA.
463 The experimental data will benefit the parameterization of vehicles emissions in
464 numerical models dealing with urban air pollution.

465 **5. Conclusions**

- 466 1. Five types of individual particles emitted by the GDI-engine vehicles were
467 identified, including soot, organic, Ca-rich, S-rich, and metal-rich particles. Among
468 them, soot, organic, and Ca-rich particles were predominant. The particles emitted
469 from GDI-engine vehicles displayed a bimodal size distribution.
- 470 2. The concentrations of the particles emitted by the GDI-engine vehicles vary with
471 different running conditions. The PM emission was the highest under the hot
472 stabilized running state, followed by those under the hot start, cold start, and
473 acceleration running states, with the emission under the idle running state being the
474 lowest under the idle running state.
- 475 3. The relative proportions of the different types of particles emitted by the GDI-
476 engine vehicles vary with different running conditions. Large amounts of organic
477 particles were emitted during hot stabilized and hot start states. Under cold start
478 and acceleration states, the emissions were enriched in soot particles. Under idle
479 state, a relatively higher number of Ca-rich particles was emitted, although the

480 absolute number was low.

481 4. After ageing in the environmental chamber, the structure of the soot particles
482 changed into a core-shell structure, and the particles were coated with condensed
483 secondary organic material. Ca-rich particles and organic particles also were
484 modified, and their content of sulfur increased after ageing.

485 5. Ageing of the emitted particles occurred rapidly, within hours. Such rapid ageing
486 could be attributable to an acid-catalyzed mechanism and to the high initial
487 concentrations of gaseous pollutants emitted by the GDI-engine gasoline.

488

489 **Data availability**

490 All data presented in this paper are available upon request. Please contact the
491 corresponding author (shaoL@cumtb.edu.cn).

492 **Author contribution**

493 LS designed this study; JX performed the experiments. JX, LS, DZ summarized
494 the data and wrote the paper. WZ, JP, WW, SS, MH supported the experiments and
495 commented the paper.

496 **Competing interests**

497 The authors declare that they have no conflict of interest.

498 **Acknowledgements**

499 This work was supported by Projects of International Cooperation and Exchanges
500 NSFC (Grant No. 41571130031). The data analysis was partly supported by Science
501 and Technology Project Founded by the Education Department of Jiangxi Province (No.

502 GJJ180226), Yue Qi Scholar Fund of China University of Mining and Technology
503 (Beijing), and a Grant-in-Aid for Scientific Research (B) (No.16H02942) from the
504 JSPS.

505 **References**

- 506 Adachi, K., and Buseck, P. R.: Changes in shape and composition of sea-salt particles upon aging in an
507 urban atmosphere, *Atmos. Environ.*, 100, 1-9, <http://dio.org/10.1016/j.atmosenv.2014.10.036>, 2015.
- 508 Alves, C. A., Lopes, D. J., Calvo, A. I., Evtyugina, M., Rocha, S., and Nunes, T.: Emissions from light-
509 duty diesel and gasoline in-use vehicles measured on chassis dynamometer test cycles, *Aerosol Air*
510 *Qual. Res.*, 15(1), 99-116, <http://dio.org/10.4209/aaqr.2014.01.0006>, 2015.
- 511 Baral, B., Raine, R., and Miskelly, G.: Effect of engine operating conditions on spark-ignition engine
512 PAH emissions, SAE Technical Paper 2011-01-1161, <http://dio.org/10.4271/2011-01-1161>, 2011.
- 513 Beardsley, R.L., and Jang, M.: Simulating the SOA formation of isoprene from partitioning and
514 aerosol phase reactions in the presence of inorganics, *Atmos Chem Phys*, 15, 33121-33159,
515 <http://dio.org/10.5194/acpd-15-33121-2015>, 2015.
- 516 Bond, T. C., Doherty, S. J., Fahey, D. W., Forster, P. M., Bernsten, T., DeAngelo, B. J., Flanner, M. G.,
517 Ghan, S., Kärcher, B., Koch, D., Kinne, S., Kondo, Y., Quinn, P. K., Sarofim, M. C., Schultz, M.
518 G., Schulz, M., Venkataraman, C., Zhang, H., Zhang, S., Bellouin, N., Guttikunda, S. K., Hopke, P.
519 K., Jacobson, M. Z., Kaiser, J. W., Klimont, Z., Lohmann, U., Schwarz, J. P., Shindell, D.,
520 Storelvmo, T., Warren, S. G., and Zender, C. S.: Bounding the role of black carbon in the climate
521 system: A scientific assessment, *J. Geophys. Res.-Atmos.*, 118(11), 5380-5552,
522 <http://dio.org/10.1002/jgrd.50171>, 2013.
- 523 Bones, D.L., Henricksen, D.K., Mang, S.A., Gonsior, M., Bateman, A.P., Nguyen, T.B., Cooper,
524 W.J., and Nizkorodov, S.A.: Appearance of strong absorbers and fluorophores in limonene-O₃
525 secondary organic aerosol due to NH⁴⁺-mediated chemical aging over long time scales, *J*
526 *Geophys Res*, 115, <http://dio.org/10.1029/2009JD012864>, 2010.
- 527 Chart-asa, C., and Gibson, J. M.: Health impact assessment of traffic-related air pollution at the urban project scale: Influence of
528 variability and uncertainty, *Sci. Total Environ.*, 506-507, 409-421,
529 <http://dio.org/10.1016/j.scitotenv.2014.11.020>, 2015.
- 530 Chang, L., Shao, L., Yang, S., Li, J., Zhang, M., Feng, X., Li, Y., 2019, Study on variation characteristics
531 of PM_{2.5} mass concentrations in Beijing after the action for comprehensive control of air pollution.
532 *Journal of Mining Science and Technology*, 2019, 4(6): 539-546. <http://dio.org/10.19606/j.cnki.jmst.2019.06.009>. (in Chinese with English Abstract)
- 534 Chart-asa, C., and Gibson, J. M.: Health impact assessment of traffic-related air pollution at the urban
535 project scale: Influence of variability and uncertainty, *Sci. Total Environ.*, 506-507, 409-421,
536 <http://dio.org/10.1016/j.scitotenv.2014.11.020>, 2015.
- 537 Chen, Z., Chen, D., Xie, X., Cai, J., Zhuang, Y., Cheng, N., He, B., and Gao, B.: Spatial self-aggregation
538 effects and national division of city-level PM_{2.5} concentrations in China based on spatio-temporal
539 clustering, *J. Clean. Prod.*, 207, 875-881, <http://dio.org/10.1016/j.jclepro.2018.10.080>, 2019.
- 540 Chen, L., Liang, Z., Zhang, X., and Shuai, S.: Characterizing particulate matter emissions from GDI and
541 PFI vehicles under transient and cold start conditions, *Fuel*, 189, 131-140,

542 <http://dio.org/10.1016/j.fuel.2016.10.055>, 2017.

543 Chen, L., and Stone, R.: Measurement of enthalpies of vaporization of isooctane and ethanol blends and
544 their effects on PM emissions from a GDI engine, *Energ. Fuel*, 25(3), 1254-1259,
545 <http://dio.org/10.1021/ef1015796>, 2011.

546 Deng, W., Hu, Q., Liu, T., Wang, X., Zhang, Y., Song, W., Sun, Y., Bi, X., Yu, J., Yang, W., Huang, X.,
547 Zhang, Z., Huang, Z., He, Q., Mellouki, A., and George, C.: Primary particulate emissions and
548 secondary organic aerosol (SOA) formation from idling diesel vehicle exhaust in China, *Sci. Total*
549 *Environ.*, 593-594, 462-469, <http://dio.org/10.1016/j.scitotenv.2017.03.088>, 2017.

550 Du, Z., Hu, M., Peng, J., Zhang, W., Zheng, J., Gu, F., Qin, Y., Yang, Y., Li, M., Wu, Y., Shao, M., and
551 Shuai, S.: Comparison of primary aerosol emission and secondary aerosol formation from gasoline
552 direct injection and port fuel injection vehicles, *Atmos. Chem. Phys.*, 18(12), 9011-9023,
553 <http://dio.org/10.5194/acp-18-9011-2018>, 2018.

554 Fu, H., Wang, Y., Li, X., and Shuai, S.: Impacts of cold-start and gasoline RON on particulate emission
555 from vehicles powered by GDI and PFI engines, SAE Technical Paper 2014-01-2836, [http://dio.org/](http://dio.org/10.4271/2014-01-2836)
556 [10.4271/2014-01-2836](http://dio.org/10.4271/2014-01-2836), 2014.

557 Fushimi, A., Kondo, Y., Kobayashi, S., Fujitani, Y., Saitoh, K., Takami, A., and Tanabe, K.:
558 Chemical composition and source of fine and nanoparticles from recent direct injection
559 gasoline passenger cars: Effects of fuel and ambient temperature, *Atmos Environ*, 124, 77-84,
560 <http://dio.org/10.1016/j.atmosenv.2015.11.017>, 2016.

561 Giechaskiel, B., Maricq, M., Ntziachristos, L., Dardiotis, C., Wang, X., Axmann, H., Bergmann, A., and
562 Schindler, W.: Review of motor vehicle particulate emissions sampling and measurement: From
563 smoke and filter mass to particle number, *J. Aerosol Sci.*, 67, 48-86,
564 <http://dio.org/10.1016/j.jaerosci.2013.09.003>, 2014.

565 Guo, S., Hu, M., Guo, Q., Zhang, X., Zheng, M., Zheng, J., Chang, C. C., Schauer, J. J., and Zhang, R.:
566 Primary sources and secondary formation of organic aerosols in Beijing, China, *Environ. Sci.*
567 *Technol.*, 18(46), 9846 - 9853, 2012.

568 Hedge, M., Weber, P., Gingrich, J., Alger, T., and Khalek, I. A.: Effect of EGR on Particle Emissions
569 from a GDI Engine, *SAE Int. J. Engines*, 4(1), 650- 666, <http://dio.org/10.4271/2011-01-0636>, 2011.

570 Hou, C., Shao, L., Hu, W., Zhang, D., Zhao, C., Xing, J., Huang, X., and Hu, M.: Characteristics
571 and aging of traffic-derived particles in a highway tunnel at a coastal city in southern China,
572 *Sci Total Environ*, 619-620, 1385-1393, <http://dio.org/10.1016/j.scitotenv.2017.11.165>, 2018.

573 Hu, W., Niu, H., Zhang, D., Wu, Z., Chen, C., Wu, Y., Shang, D., and Hu, M.: Insights into a dust event
574 transported through Beijing in spring 2012: Morphology, chemical composition and impact on
575 surface aerosols, *Sci. Total Environ.*, 565, 287-298, <http://dio.org/10.1016/j.scitotenv.2016.04.175>,
576 2016.

577 Huang, R., Zhang, Y., Bozzetti, C., Ho, K., Cao, J., Han, Y., Daellenbach, K. R., Slowik, J. G., Platt, S.
578 M., Canonaco, F., Zotter, P., Wolf, R., Pieber, S. M., Bruns, E. A., Crippa, M., Ciarelli, G.,
579 Piazzalunga, A., Schwikowski, M., Abbaszade, G., Schnelle-Kreis, J., Zimmermann, R., An, Z.,
580 Szidat, S., Baltensperger, U., Haddad, I. E., and Prévôt, A. S. H.: High secondary aerosol
581 contribution to particulate pollution during haze events in China, *Nature*, 514(7521), 218-222,
582 <http://dio.org/10.1038/nature13774>, 2014.

583 Hwa, M., and Yu, T.: Development of real-world driving cycles and estimation of emission factors
584 for in-use light-duty gasoline vehicles in urban areas, *Environ Monit Assess*, 186, 3985-3994,
585 <http://dio.org/10.1007/s10661-014-3673-1>, 2014.

586 Jacobson, M. Z.: Strong radiative heating due to the mixing state of black carbon in atmospheric aerosols,
587 Nature, 409(6821), 695-697, <http://dio.org/10.1038/35055518>, 2001.

588 Jang, M. S., Czoschke, N. M., Lee, S., and Kamens, R. M.: Heterogeneous atmospheric aerosol
589 production by acid-catalyzed particle-phase reactions, Science, 298(5594), 814-817,
590 <http://dio.org/10.1126/science.1075798>, 2002.

591 Jang, M., Czoschke, N. M., and Northcross, A. L.: Atmospheric organic aerosol production by
592 heterogeneous acid-catalyzed reactions, Chemphyschem, 5(11), 1647-1661,
593 <http://dio.org/10.1002/cphc.200301077>, 2004.

594 Jathar, S. H., Gordon, T. D., Hennigan, C. J., Pye, H. O. T., Pouliot, G., Adams, P. J., Donahue, N. M.,
595 and Robinson, A. L.: Unspeciated organic emissions from combustion sources and their influence
596 on the secondary organic aerosol budget in the United States, P. Natl. Acad. Sci. USA, 111(29),
597 10473-10478, <http://dio.org/10.1073/pnas.1323740111>, 2014.

598 Kanakidou, M., Seinfeld, J. H., Pandis, S. N., Barnes, I., Dentener, F. J., Facchini, M. C., Van Dingenen,
599 R., Ervens, B., Nenes, A., Nielsen, C. J., Swietlicki, E., Putaud, J. P., Balkanski, Y., Fuzzi, S., Horth,
600 J., Moortgat, G. K., Winterhalter, R., Myhre, C., Tsigaridis, K., Vignati, E., Stephanou, E. G., and
601 Wilson, J.: Organic aerosol and global climate modelling: A review, Atmos. Chem. Phys., 5, 1053-
602 1123, <http://dio.org/10.5194/acp-5-1053-2005>, 2005.

603 Khalek, I. A., Bougher, T., and Jetter, J. J.: Particle Emissions from a 2009 gasoline direct injection
604 engine using different commercially available fuels, SAE Int. J. Fuels Lubr., 3(2), 623- 637,
605 <http://dio.org/10.4271/2010-01-2117>, 2010.

606 Kuwata, M., Liu, Y., McKinney, K., and Martin, S.T.: Physical state and acidity of inorganic sulfate
607 can regulate the production of secondary organic material from isoprene photooxidation
608 products, Phys Chem Chem Phys: PCCP, 17, 5670-5678, <http://dio.org/10.1039/C4CP04942J>,
609 2015.

610 Lack, D.A., Langridge, J.M., Bahreini, R., Cappa, C.D., Middlebrook, A.M., and Schwarz, J.P.:
611 Brown carbon and internal mixing in biomass burning particles, P Natl Acad Sci USA, 109,
612 <http://dio.org/14802-14807>, 10.1073/pnas.1206575109, 2012.

613 Lambe, A.T., Ahern, A.T., Wright, J.P., Croasdale, D.R., Davidovits, P., and Onasch, T.B.:
614 Oxidative aging and cloud condensation nuclei activation of laboratory combustion soot, J
615 Aerosol Sci, 79, 31-39, <http://dio.org/10.1016/j.jaerosci.2014.10.001>, 2015.

616 Lang-Yona, N., Abo-Riziq, A., Erlick, C., Segre, E., Trainic, M., and Rudich, Y.: Interaction of
617 internally mixed aerosols with light, Phys Chem Chem Phys, 12, 21-31,
618 <http://dio.org/10.1039/B913176K>, 2010.

619 Laskin, A., Laskin, J., and Nizkorodov, S.A.: Chemistry of Atmospheric Brown Carbon, Chem Rev,
620 115, 4335-4382, <http://dio.org/10.1021/cr5006167>, 2015.

621 Li, W., and Shao, L.: Transmission electron microscopy study of aerosol particles from the brown hazes
622 in northern china, J. Geophys. Res.-Atmos., <http://dio.org/D09302>, 2009.

623 Liati, A., Schreiber, D., Dasilva, Y. A. R., and Eggenchwiler, P. D.: Ultrafine particle emissions from
624 modern gasoline and diesel vehicles: An electron microscopic perspective, Environ. Pollut., 239,
625 661-669, <http://dio.org/10.1016/j.envpol.2018.04.081>, 2018.

626 Liu, L., Kong, S., Zhang, Y., Wang, Y., Xu, L., Yan, Q., Lingaswamy, A. P., Shi, Z., Lv, S., Niu, H.,
627 Shao, L., Hu, M., Zhang, D., Chen, J., Zhang, X., and Li, W.: Morphology, composition, and mixing
628 state of primary particles from combustion sources - crop residue, wood, and solid waste, Sci. Rep.-
629 UK, <http://dio.org/10.1038/s41598-017-05357-2>, 2017.

630 Loh, N.D., Hampton, C.Y., Martin, A.V., Starodub, D., Sierra, R.G., Barty, A., Aquila, A., Schulz,
631 J., Lomb, L., Steinbrener, J., Shoeman, R.L., Kassemeyer, S., Bostedt, C., Bozek, J., Epp, S.W.,
632 Erk, B., Hartmann, R., Rolles, D., Rudenko, A., Rudek, B., Foucar, L., Kimmel, N.,
633 Weidenspointner, G., Hauser, G., Holl, P., Pedersoli, E., Liang, M., Hunter, M.M., Gumprecht,
634 L., Coppola, N., Wunderer, C., Graafsma, H., Maia, F.R.N.C., Ekeberg, T., Hantke, M.,
635 Fleckenstein, H., Hirsemann, H., Nass, K., White, T.A., Tobias, H.J., Farquar, G.R., Benner,
636 W.H., Hau-Riege, S.P., Reich, C., Hartmann, A., Soltau, H., Marchesini, S., Bajt, S.,
637 Barthelmess, M., Bucksbaum, P., Hodgson, K.O., Strueder, L., Ullrich, J., Frank, M.,
638 Schlichting, I., Chapman, H.N., and Bogan, M.J.: Fractal morphology, imaging and mass
639 spectrometry of single aerosol particles in flight, *Nature*, 486, 513-517,
640 <http://dio.org/10.1038/nature11222>, 2012.

641 Lu, K.D., Hofzumahaus, A., Holland, F., Bohn, B., Brauers, T., Fuchs, H., Hu, M., Häseler, R., Kita,
642 K., Kondo, Y., Li, X., Lou, S.R., Oebel, A., Shao, M., Zeng, L.M., Wahner, A., Zhu, T., Zhang,
643 Y.H., and Rohrer, F.: Missing OH source in a suburban environment near Beijing: observed
644 and modelled OH and HO₂ concentrations in summer 2006, *Atmos Chem Phys*, 13, 1057-1080,
645 <http://dio.org/10.5194/acp-13-1057-2013>, 2013.

646 Luo, Y., Zhu, L., Fang, J., Zhuang, Z., Guan, C., Xia, C., Xie, X., and Huang, Z.: Size distribution,
647 chemical composition and oxidation reactivity of particulate matter from gasoline direct injection
648 (GDI) engine fueled with ethanol-gasoline fuel, *Appl. Therm. Eng.*, 89, 647-655,
649 <http://dio.org/10.1016/j.applthermaleng.2015.06.060>, 2015.

650 Ma, Q., Wu, Y., Zhang, D., Wang, X., Xia, Y., Liu, X., Tian, P., Han, Z., Xia, X., Wang, Y., and
651 Zhang, R.: Roles of regional transport and heterogeneous reactions in the PM_{2.5} increase during
652 winter haze episodes in Beijing, *Sci Total Environ*, 599, 246-253,
653 <http://dio.org/10.1016/j.scitotenv.2017.04.193>, 2017.

654 Maricq, M. M., Szente, J., Loos, M., and Vogt, R.: Motor vehicle PM emissions measurement at LEV
655 III levels, *SAE Int. J. Engines*, 4(1), 597- 609, <http://dio.org/10.4271/2011-01-0623>, 2011.

656 Mauldin, R. L. I., Berndt, T., Sipilae, M., Paasonen, P., Petaja, T., Kim, S., Kurten, T., Stratmann, F.,
657 Kerminen, V., and Kulmala, M.: A new atmospherically relevant oxidant of sulphur dioxide, *Nature*,
658 488(7410), 193-196, <http://dio.org/10.1038/nature11278>, 2012.

659 National Bureau of Statistics of China, 2018. China Statistical Yearbook 2018, part sixteen:
660 Transportation, post and telecommunications and software industry. Available on line at:
661 <http://www.stats.gov.cn/tjsj/ndsj/2018/indexch.htm>, 2018.

662 Niu, H., Cheng, W., Hu, W., and Pian, W.: Characteristics of individual particles in a severe short-period
663 haze episode induced by biomass burning in Beijing, *Atmos. Pollut. Res.*, 7(6), 1072-1081,
664 <http://dio.org/10.1016/j.apr.2016.05.011>, 2016.

665 Niu, H., Hu, W., Zhang, D., Wu, Z., and Guo, S.: Variations of fine particle physiochemical
666 properties during a heavy haze episode in the winter of Beijing, *Sci Total Environ*, 571, 103-
667 109, <http://dio.org/10.1016/j.scitotenv.2016.07.147>, 2016.

668 Niu, H., Shao, L., and Zhang, D.: Aged status of soot particles during the passage of a weak cyclone in
669 Beijing, *Atmos. Environ.*, 45(16), 2699-2703, <http://dio.org/10.1016/j.atmosenv.2011.02.056>, 2011.

670 Okada, K., Qin, Y., and Kai, K.: Elemental composition and mixing properties of atmospheric mineral
671 particles collected in Hohhot, China, *Atmos. Res.*, 73(1-2), 45-67,
672 <http://dio.org/10.1016/j.atmosres.2004.08.001>, 2005.

673 Peng, J., Hu, M., Guo, S., Du, Z., Shang, D., Zheng, J., Zheng, J., Zeng, L., Shao, M., Wu, Y., Collins,

674 D., and Zhang, R.: Ageing and hygroscopicity variation of black carbon particles in Beijing
675 measured by a quasi-atmospheric aerosol evolution study (QUALITY) chamber, *Atmos. Chem.*
676 *Phys.*, 17(17), 10333-10348, <http://dio.org/10.5194/acp-17-10333-2017>, 2017.

677 Peng, J.F., Hu, M., Wang, Z.B., Huang, X.F., Kumar, P., Wu, Z.J., Guo, S., Yue, D.L., Shang, D.J.,
678 Zheng, Z., and He, L.Y.: Submicron aerosols at thirteen diversified sites in China: size distribution,
679 new particle formation and corresponding contribution to cloud condensation nuclei production,
680 *Atmos Chem Phys*, 14, 10249-10265, [10.5194/acp-14-10249-2014](http://dio.org/10.5194/acp-14-10249-2014), 2014.

681 Petzold, A., Marsh, R., Johnson, M., Miller, M., Sevcenco, Y., Delhaye, D., Ibrahim, A., Williams, P.,
682 Bauer, H., Crayford, A., Bachalo, W. D., and Raper, D.: Evaluation of methods for measuring
683 particulate matter emissions from gas turbines, *Environ. Sci. Technol.*, 45(8), 3562-3568, 2011.

684 Rönkkö, T., Lähde, T., Heikkilä, J., Pirjola, L., Bauschke, U., Arnold, F., Schlager, H., Rothe, D., Yli-
685 Ojanperä, J., and Keskinen, J.: Effects of gaseous sulphuric acid on diesel exhaust nanoparticle
686 formation and characteristics, *Environ. Sci. Technol.*, 47(20), 11882-11889,
687 <http://dio.org/10.1021/es402354y>, 2013.

688 Scott, C. E., Rap, A., Spracklen, D. V., Forster, P. M., Carslaw, K. S., Mann, G. W., Pringle, K. J.,
689 Kivekas, N., Kulmala, M., Lihavainen, H., and Tunved, P.: The direct and indirect radiative effects
690 of biogenic secondary organic aerosol, *Atmos. Chem. Phys.*, 14(1), 447-470,
691 <http://dio.org/10.5194/acp-14-447-2014>, 2014.

692 Shao, L., Hu, Y., Fan, J., Wang, J., Wang, J., and Ma, J.: Physicochemical characteristics of aerosol
693 particles in the Tibetan Plateau: Insights from TEM-EDX analysis, *J. Nanosci. Nanotechnol.*, 17(9),
694 6899-6908, <http://dio.org/10.1166/jnn.2017.14472>, 2017.

695 Shao, L., Hu, Y., Shen, R., Schäfer, K., Wang, J., Wang, J., Schnelle-Kreis, J., Zimmermann, R., Bérubé,
696 K., and Suppan, P.: Seasonal variation of particle-induced oxidative potential of airborne particulate
697 matter in Beijing, *Sci. Total Environ.*, 579, 1152-1160,
698 <http://dio.org/10.1016/j.scitotenv.2016.11.094>, 2017.

699 Song, C., Na, K., Warren, B., Malloy, Q., and Cocker, D.R.: Secondary Organic Aerosol Formation from
700 m-Xylene in the Absence of NO_x, *Environ Sci Technol*, 41, 7409-7416,
701 <http://dio.org/10.1021/es070429r>, 2007.

702 Song, M., Zhang, C., Wu, H., Mu, Y., Ma, Z., Zhang, Y., Liu, J., and Li, X.: The influence of OH
703 concentration on SOA formation from isoprene photooxidation, *Sci Total Environ*, 650, 951-957,
704 <http://dio.org/10.1016/j.scitotenv.2018.09.084>, 2019.

705 Shi, Z., Vu, T., Kotthaus, S., Harrison, R. M., Grimmond, S., Yue, S., Zhu, T., Lee, J., Han, Y., Demuzere,
706 M., Dunmore, R. E., Ren, L., Liu, D., Wang, Y., Wild, O., Allan, J., Acton, W. J., Barlow, J., Barratt,
707 B., Beddows, D., Bloss, W. J., Calzolari, G., Carruthers, D., Carslaw, D. C., Chan, Q., Chatzidiakou,
708 L., Chen, Y., Crilley, L., Coe, H., Dai, T., Doherty, R., Duan, F., Fu, P., Ge, B., Ge, M., Guan, D.,
709 Hamilton, J. F., He, K., Heal, M., Heard, D., Hewitt, C. N., Hollaway, M., Hu, M., Ji, D., Jiang, X.,
710 Jones, R., Kalberer, M., Kelly, F. J., Kramer, L., Langford, B., Lin, C., Lewis, A. C., Li, J., Li, W.,
711 Liu, H., Liu, J., Loh, M., Lu, K., Lucarelli, F., Mann, G., McFiggans, G., Miller, M. R., Mills, G.,
712 Monk, P., Nemitz, E., O'Connor, F., Ouyang, B., Palmer, P. I., Percival, C., Popoola, O., Reeves,
713 C., Rickard, A. R., Shao, L., Shi, G., Spracklen, D., Stevenson, D., Sun, Y., Sun, Z., Tao, S., Tong,
714 S., Wang, Q., Wang, W., Wang, X., Wang, X., Wang, Z., Wei, L., Whalley, L., Wu, X., Wu, Z.,
715 Xie, P., Yang, F., Zhang, Q., Zhang, Y., Zhang, Y., and Zheng, M.: Introduction to the special issue
716 "In-depth study of air pollution sources and processes within Beijing and its surrounding region
717 (APHH-Beijing)", *Atmos. Chem. Phys.*, 19(11), 7519-7546, [http://dio.org/10.5194/acp-19-7519-](http://dio.org/10.5194/acp-19-7519-2019)

718 2019, 2019.

719 Suarez-Bertoa, R., Zardini, A. A., Platt, S. M., Hellebust, S., Pieber, S. M., El Haddad, I., Temime-
720 Roussel, B., Baltensperger, U., Marchand, N., Prévôt, A. S. H., and Astorga, C.: Primary emissions
721 and secondary organic aerosol formation from the exhaust of a flex-fuel (ethanol) vehicle, *Atmos.*
722 *Environ.*, 117, 200-211, <http://dio.org/10.1016/j.atmosenv.2015.07.006>, 2015.

723 Szybist, J. P., Youngquist, A. D., Barone, T. L., Storey, J. M., and Moore, W. R.: Ethanol blends and
724 engine operating strategy effects on light-duty spark-ignition engine particle emissions, *Energ. Fuel.*,
725 25(11), 4977-4985, <http://dio.org/10.1021/ef201127y>, 2011.

726 Wang, W., Shao, L., Li, J., Chang, L., Zhang, D., Zhang, C., and Jiang, J.: Characteristics of individual
727 particles emitted from an experimental burning chamber with coal from the lung cancer area of
728 Xuanwei, China, *Aerosol Air Qual. Res.*, 19(2), 355-363, <http://dio.org/10.4209/aaqr.2018.05.0187>,
729 2019.

730 Xing, J., Shao, L., Zhang, W., Peng, J., Wang, W., Hou, C., Shuai, S., Hu, M., and Zhang, D.:
731 Morphology and composition of particles emitted from a port fuel injection gasoline vehicle under
732 real-world driving test cycles, *J. Environ. Sci-China*, 76, 339-348,
733 <http://dio.org/10.1016/j.jes.2018.05.026>, 2019.

734 Xing, J., Shao, L., Zheng, R., Peng, J., Wang, W., Guo, Q., Wang, Y., Qin, Y., Shuai, S., and Hu, M.:
735 Individual particles emitted from gasoline engines: Impact of engine types, engine loads and fuel
736 components, *J. Clean. Prod.*, 149, 461-471, <http://dio.org/10.1016/j.jclepro.2017.02.056>, 2017.

737 Yu, L., Wang, G., Zhang, R., Zhang, L., Song, Y., Wu, B., Li, X., An, K., and Chu, J.: Characterization
738 and source apportionment of PM_{2.5} in an urban environment in Beijing, *Aerosol Air Qual. Res.*,
739 13(2), 574-583, 2013.

740 Zhang, H., Cheng, S., Li, J., Yao, S., and Wang, X.: Investigating the aerosol mass and chemical
741 components characteristics and feedback effects on the meteorological factors in the
742 Beijing-Tianjin-Hebei region, China, *Environ. Pollut.*, 244, 495-502,
743 <http://dio.org/10.1016/j.envpol.2018.10.087>, 2019.

744 Zhang, M., Li, Z., Xu, M., Yue, J., Cai, Z., Yung, K.K.L., and Li, R.: Pollution characteristics,
745 source apportionment and health risks assessment of fine particulate matter during a
746 typical winter and summer time period in urban Taiyuan, China, *Hum Ecol Risk Assess.*,
747 <http://dio.org/10.1080/10807039.2019.1684184>, 2019.

748 Zhang, Y., Yuan, Q., Huang, D., Kong, S., Zhang, J., Wang, X., Lu, C., Shi, Z., Zhang, X., Sun, Y.,
749 Wang, Z., Shao, L., Zhu, J., and Li, W.: Direct observations of fine primary particles from residential
750 coal burning: Insights into their morphology, composition, and hygroscopicity, *J. Geophys. Res.-*
751 *Atmos.*, 123(22), 12,964-12,979, <http://dio.org/10.1029/2018JD028988>, 2018.

752 Zhu, J., Penner, J. E., Lin, G., Zhou, C., Xu, L., and Zhuang, B.: Mechanism of SOA formation
753 determines magnitude of radiative effects, *P. Natl. Acad. Sci. USA*, 114(48), 12685-12690,
754 <http://dio.org/10.1073/pnas.1712273114>, 2017.

755 Zimmerman, N., Wang, J. M., Jeong, C., Ramos, M., Hilker, N., Healy, R. M., Sabaliauskas, K., Wallace,
756 J. S., and Evans, G. J.: Field measurements of gasoline direct injection emission factors: Spatial and
757 seasonal variability, *Environ. Sci. Technol.*, 50(4), 2035-2043,
758 <http://dio.org/10.1021/acs.est.5b04444>, 2016.

759

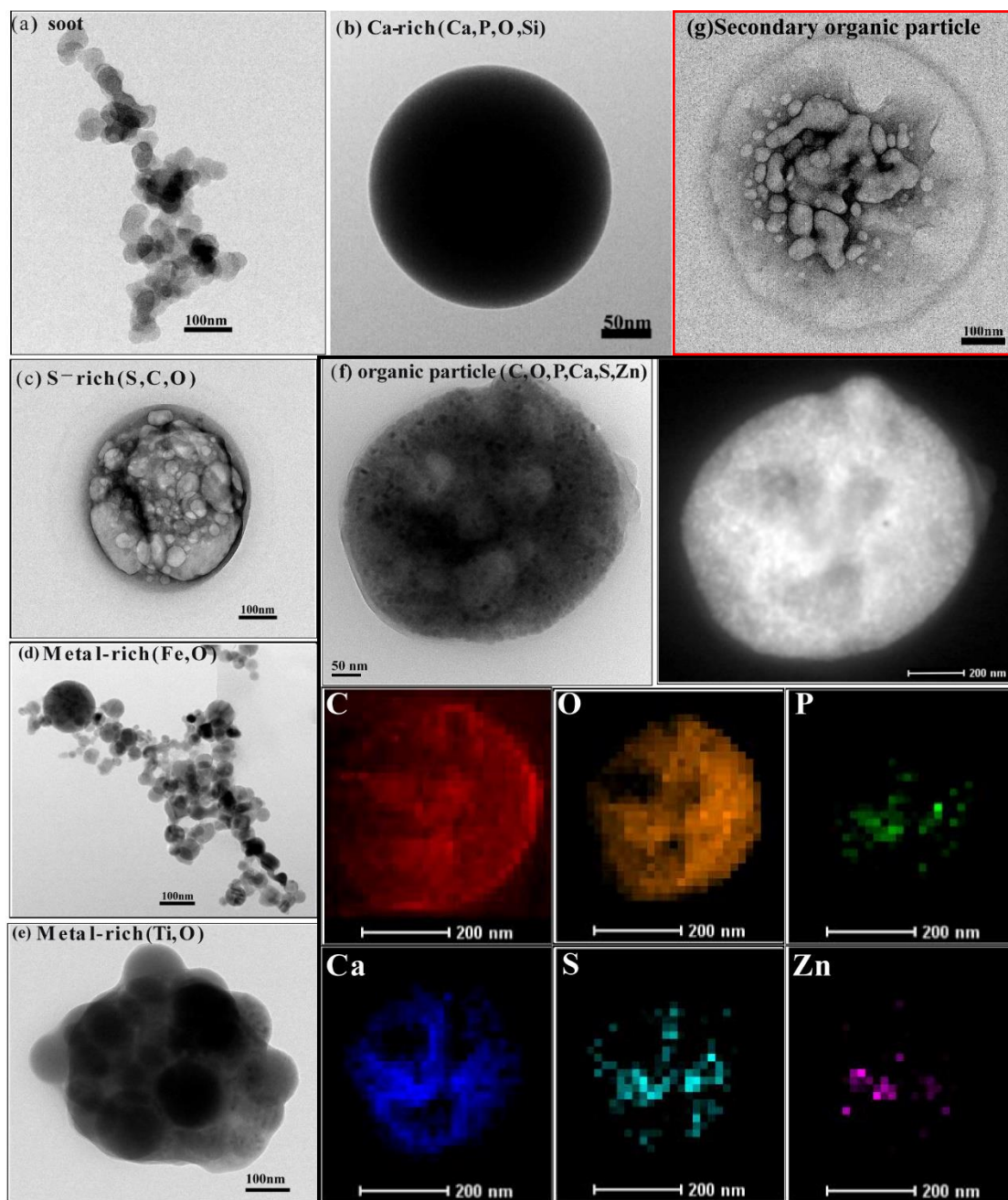
760 **List of tables:**761 Table 1 Comparison of chemical components between various sources including fossil
762 fuels, biomass burning and urban waste burning

Study	Source	Particle of type and relative percentages	Chemical composition of organic particles
This study	GDI-engine vehicles	Organic particles (OM) (32%), Soot (32%), Ca-rich particles (26%), S-rich (5%) and metal-containing particles (4%)	OM with Ca and weak P, S, and Zn
Xing et al. (2019)	PFI-engine vehicles	OM (44%), soot (23%), Ca-rich particles (20%), S-rich (6%) and metal-containing particles (6%).	OM with Ca and weak P, S, and Zn.
Liati et al. (2018)	GDI, PFI and diesel vehicles	Soot, OM (called ash-bearing soot particles) and ash particles.	OM with Ca, S, P, Fe and minor Zn.
Liu et al. (2017)	Crop residue combustion	OM (27%), OM-K (43%), OM-soot-K (27%), soot-OM (3%).	OM particles with K content.
Liu et al. (2017)	Wood combustion	OM (16%), soot (18%), OM-K (22%), OM-soot-K (15%), soot-OM (29%).	OM particles with K content.
Wang et al. (2019)	Coal burning	OM (38%), soot (40%), S-rich particles (2%), and mineral particles (18%).	OM mainly consisted of C, O and Si.
Zhang et al. (2018)	Residential coal burning	OM (51%), OM-S (24%), soot-OM (23%), S-rich (1%), metal-rich particles (1%), mineral particles (1%).	OM contained C, O, and Si with minor amounts of S and Cl.

763

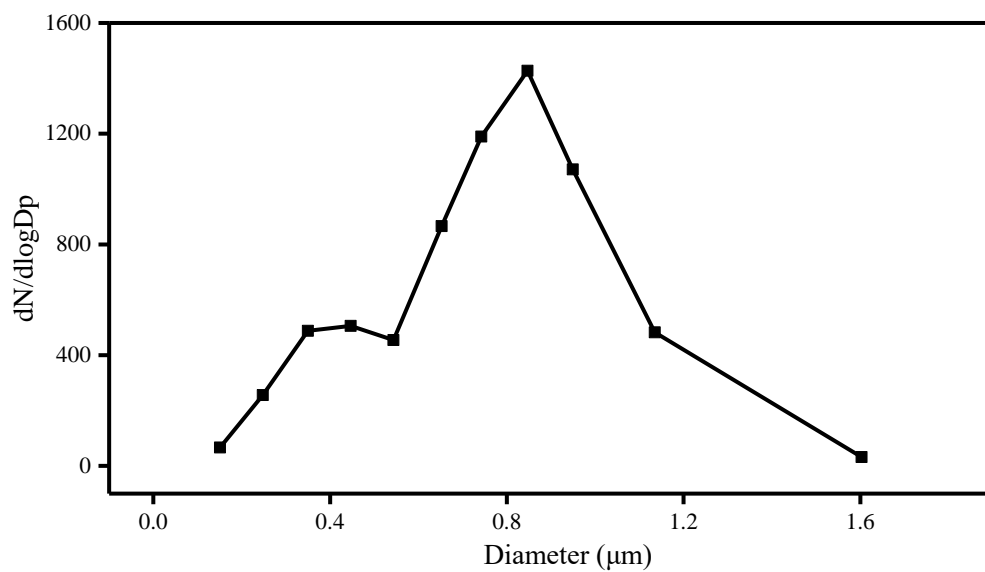
764

765 **List of figures:**



766

767 Figure 1. TEM images of the individual primary particles emitted from the GDI-engine
 768 gasoline vehicle and the secondary organic particle in the chamber after exposure to
 769 ambient sunlight for 3.5 hours. (a) soot particle; (b) Ca-rich particle; (c) S-rich particles;
 770 (d) Metal-rich particles (Fe); (e) Metal-rich particles (Ti); (f) bright-field-TEM and
 771 dark-field-TEM image of organic particles, and others are the mapping of the C, O, P,
 772 Ca, S, and Zn in the organic particle; (g) secondary organic particle in chamber.
 773



774

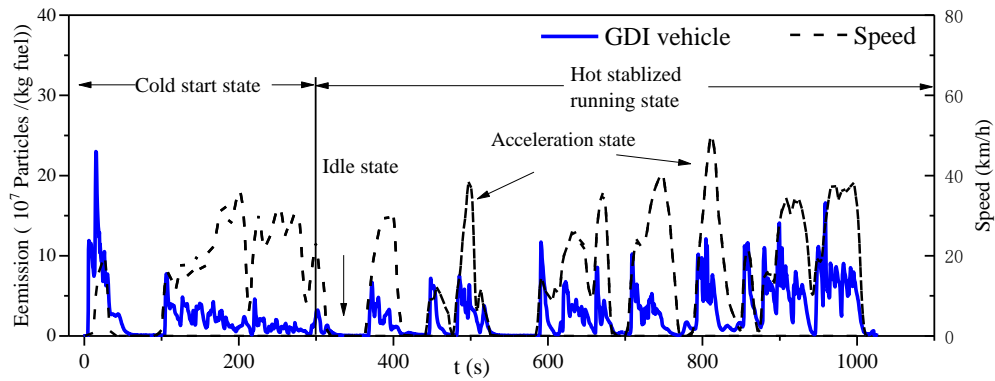
775 Figure 2. Size distribution of analyzed particles emitted from the GDI-engine gasoline
776 vehicles by the TEM images. In total, 2880 particles were analyzed from the GDI-
777 engine vehicles. Particles smaller than 0.25 μm should have been underestimated
778 because of the collection efficiency of the impactor.

779

780

781

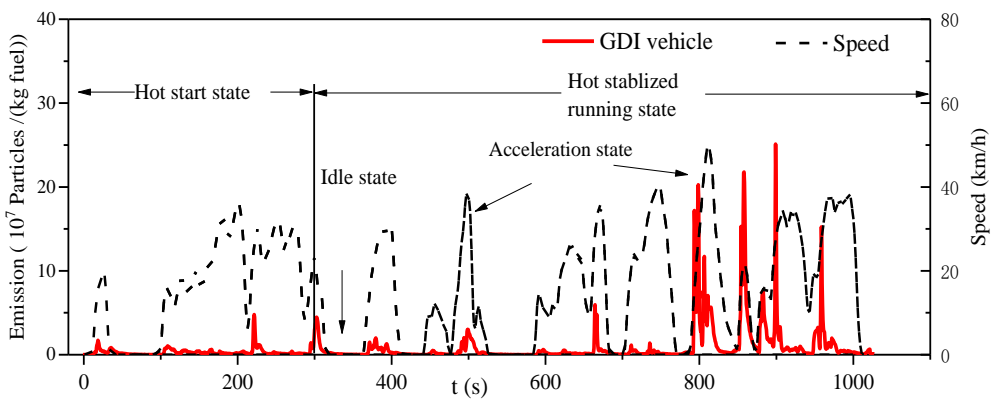
(a)



782

783

(b)

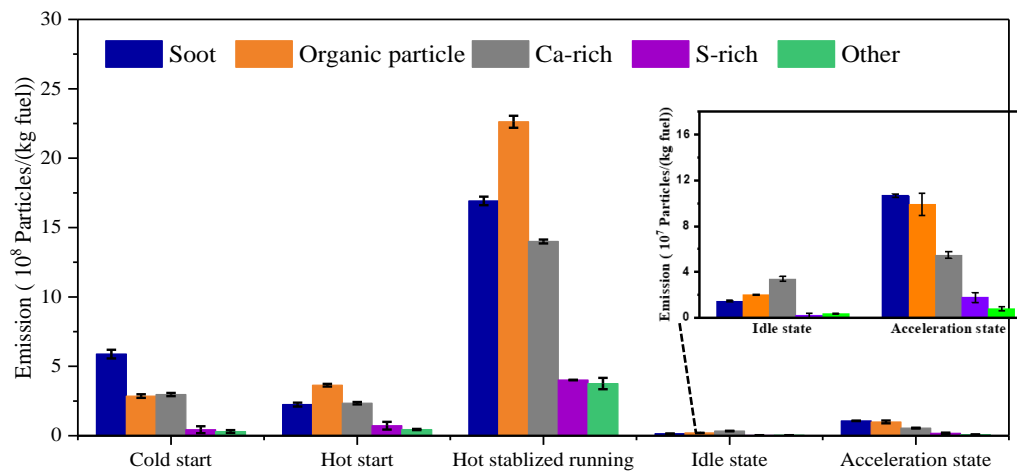


784

785 Figure 3. Particles in accumulation mode from the GDI vehicle during cold start (a) and
786 hot start (b) driving cycle. The vehicle speed is also shown for reference. Before the
787 test with cold start, the temperatures of the engine coolant and oil could not differ by
788 more than $2\text{ }^{\circ}\text{C}$ during the soak temperature. The hot start test was conducted within 5
789 mins after the cold start test. The number concentration of particles during the tests was
790 monitored by DMS 500.

791

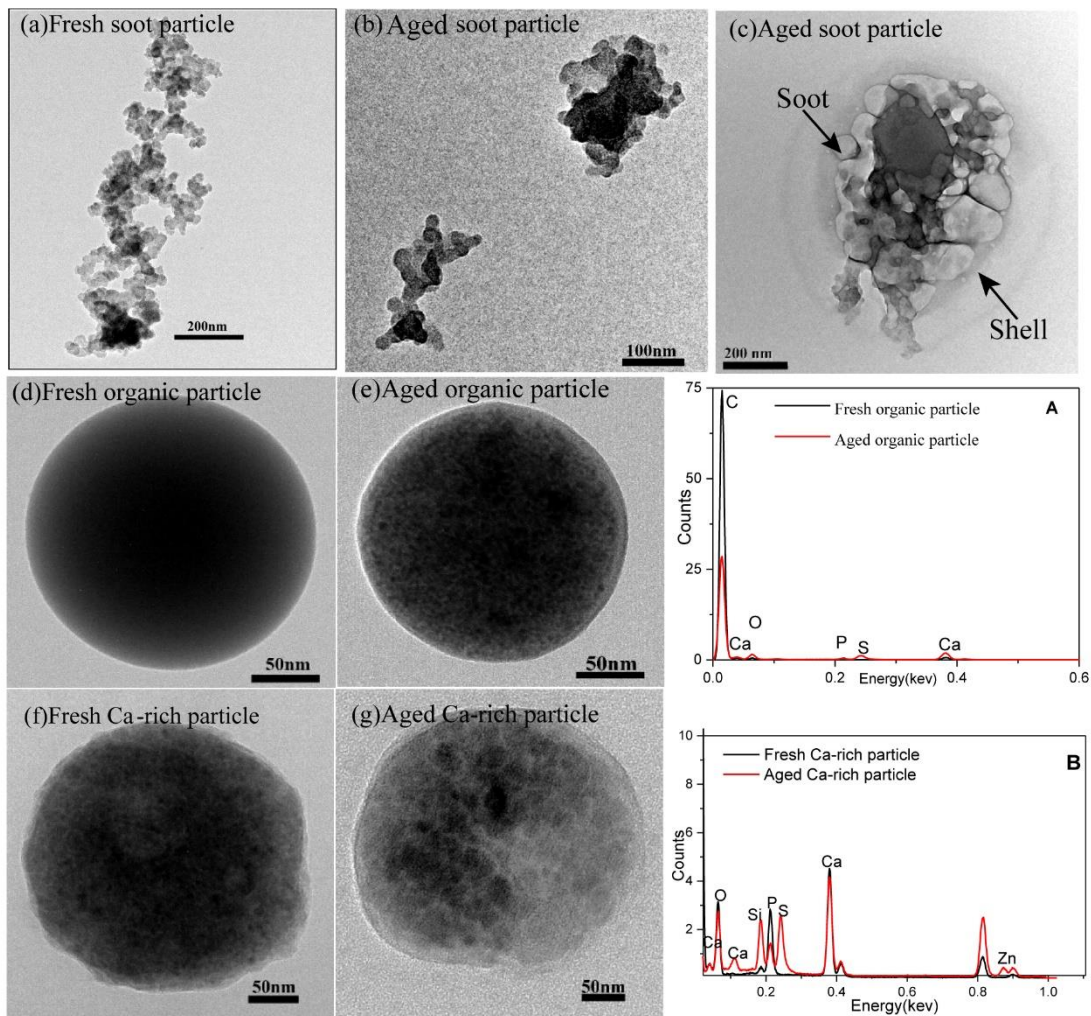
792



794

795 Figure 4. The number of different type particles in the emissions from the GDI vehicle
 796 under the different running states by the burning of per unit of fuel, including cold start,
 797 hot start, hot stabilization, idle, and acceleration states. Data presented as
 798 mean \pm standard deviation, N = 3.

799



800

801 Figure 5. TEM images of particles in the chamber after exposure to ambient sunlight
 802 for 3.5 hours. (a) Fresh soot particles; (b) Aged soot particles; (c) Aged soot particle (d)
 803 Fresh organic particle (e) Aged organic particle (f) Fresh Ca-rich particle (g) Aged Ca-
 804 rich particle (A) EDX spectrum for a fresh organic particle and an aged organic particle.
 805 (B) EDX spectrum for a fresh organic particle and an aged Ca-rich particle.
 806